Appl. Phys. B 52, 195–199 (1991)

Applied Physics B Photophysics and Laser Chemistry

Rapid Discharge-Pumped Wide Aperture X-ray Preionized KrF Laser

H. Mizoguchi*, A. Endoh, J. Jethwa, B. Rácz, and F. P. Schäfer**

Max-Planck-Institut für biophysikalische Chemie, Abteilung Laserphysik, Postfach 28 41, W-3400 Göttingen, Fed. Rep. Germany

Received 15 May 1990/Accepted 25 October 1990

Abstract. A wide aperture X-ray preionized discharge-pumped KrF excimer laser has been constructed. A flat plate pulse-forming line (36 nF, 340 kV) charges a peaking capacitor (6 nF) through a rail-gap to facilitate a rapid discharge in the laser head. Collimated X-ray preionization is employed to obtain a wide and uniform discharge. The laser is intended to be used as a short pulse amplifier and results are presented when characterized as an oscillator. The active cross-section of the laser beam is 10×8 cm^2 with 50 cm effective electrode length. The laser pulse energy exceeds 4.7 J in a 28 ns pulse (FWHM).

PACS: 42.55G, 42.60B, 52.80H

Intensive efforts are currently being directed toward the construction of wide aperture excimer lasers to be used as amplifiers in high power (more than 1 TW) short pulse generation systems [1, 2]. These systems are applicable to multiphoton phenomena, excitation source of X-ray lasers, nuclear physics, etc.

It is known that the properties of KrF amplification are markedly better than those of XeCl in the short pulse (subpicosecond) region [3]. Therefore wide-aperture KrF amplifiers have been developed in several high power short pulse generation systems [1, 4]. Spatially uniform gain distribution over a wide aperture is desirable because of the saturation property of the amplifier and ease of fit to axially symmetrical optics. From the practical point of view, a small signal gain coefficient of 3% cm^{-1} at a gain time window of approximately 30 ns and repetition rate capability of 1 Hz are desirable for the KrF subpicosecond amplifier.

Most wide-aperture (more than 10×10 cm^2) KrF excimer lasers have used *e*-beam pumping instead of discharge excitation because of scalability and beam homogeneity. However, the discharge approach has the advantage of high repetition rate capability, compactness, easy maintenance and operation. The scalability to increase the active area of discharge-pumped excimer laser is somewhat limited, because the pumping power is decreased in a wider discharge gap chamber mainly by the inevitable increase in laser head inductance [5]. Especially in the case of discharge-pumped KrF excimer lasers, the requirement of pumping power is higher than that of XeCl excimer lasers. Hence the discharge-pumped wide-aperture KrF excimer laser is more difficult to realize than the XeCl excimer laser [6]. Up to now several wide beam KrF lasers have been demonstrated, for example, 6×5 cm^2 by X-ray preionization [7], 7×6 cm^2 by UV preionization [6]. We report here on a 10×8 cm^2 active aperture X-ray preionized discharge-pumped KrF excimer laser designed for subpicosecond pulse amplification.

1. Experimental

The laser schematic is shown in Fig. 1. A rapid rise of both voltage [8] and current [9] is important to realize a spatially wide discharge. Large scale discharge-pumped excimer laser devices have used the combination of pulse-forming lines (PFL) and rail-gap switches for the driving circuits [10]. However, to further decrease the current risetime, we have used an additional peaking capacitor (6 nF, 0.8 Ω) charged by a water dielectric double parallel-plate PFL (36 nF, 0.8 Ω) through a rail-gap switch for the main discharge. As the X-ray preionization source, a water-capacitor (8 nF) driven vacuum diode is used [11]. The two storage capacitors, namely the pulse-forming line and the water capacitor for the X-ray gun, are negatively

Permanent addresses: *Komatsu Ltd., Research Division, Laser Develop Dept., Manda 1200, Hiratsuka-shi, Kanagawa 254, Japan
** JATE University, Research Group on Laser Physics of the Hungarian Academy of Sciences, Dóm tér 9, H-6720 Szeged, Hungary

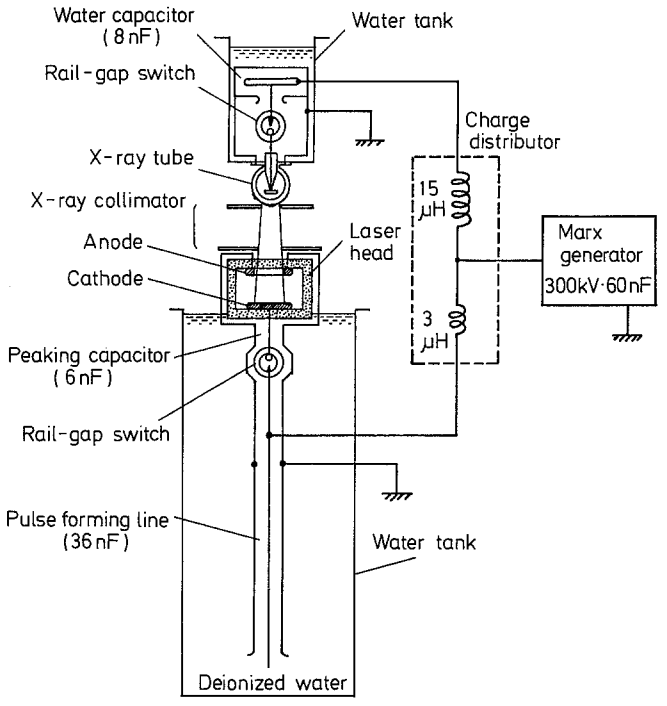

Fig. 1. Schematic of the laser head, pulsed power module, and X-ray preionizer

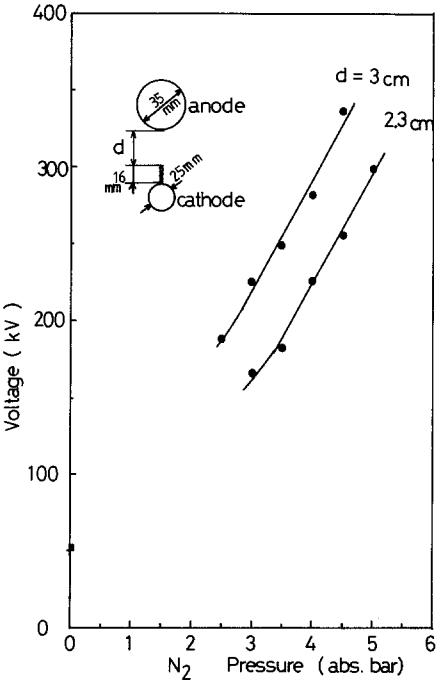

Fig. 2. Dependence of the self-breakdown voltage on pressure in the rail-gap switches

pulse-charged simultaneously by a single Marx-generator through an inductive charge distributor.

The primary energy storage source is a SF_6-insulated 5-stage Marx-generator (300 nF/75 kV per stage) of a negative polarity output with a maximum repetition rate capability of 1 Hz. After the charging of the water capacitors by the Marx generator, the X-ray gun is ignited via a multichannel rail-gap switch [12] and the discharge region in the laser head is thus preionized by the resulting X-ray emission. Approximately 100 ns after firing of the X-ray gun, a second rail-gap switch for the main discharge is fired. The charge stored in the PFL is transferred to the peaking water capacitor (6 nF). The main laser discharge now starts in the preionized region. The timing between the two rail-gap switches can be changed with the operational pressure of the switches and the inductance ratio of the charge distributor situated in the Marx enclosure.

The basic design of the X-ray diode originated from [14]. The housing is made from 5 mm thick aluminum cylinder of 150 mm diameter. A transmission geometry with a Ta foil anode and $2 \times 40\ cm^2$ carbon-felt cold-cathode is used. The cathode is held by three parallel high voltage feed-throughs and the anode–cathode separation is 15 mm. The cathode is connected to the energy storage water capacitor (8 nF) via a rail-gap switch with 23 mm electrode separation. For 300 kV hold off at the water capacitor, we use 5 bar N_2 gas as shown in Fig. 2. The number of arc channels is 4–5, and the jitter of the rail-gap switch is less than 20 ns in the self-breakdown mode. The typical X-ray dose with the water capacitor charged to 300 kV is about 1 R at the top of the laser head which is situated 16 cm away from the X-ray gun anode.

In the oscillator mode experiments, where precise synchronization is not necessary, we operate the rail-gap

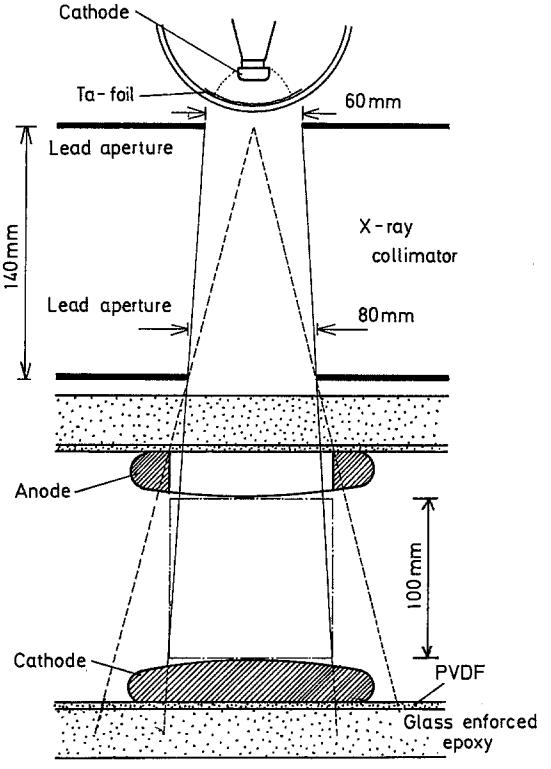

Fig. 3. Cross-section of the laser head and the collimated X-ray preionization

switches with edge-rod electrodes geometry in the self-breakdown mode. In Fig. 2 the self-breakdown voltage dependence on gas pressure is shown. The main discharge rail-gap has a separation of 30 mm between the edge and rod. The performance of this rail-gap is similar to that used for the X-ray generation. Laser triggering of the rail-

gap can be used to reduce the jitter for precise timing in subpicosecond amplification experiments [13].

The cross-section of the laser head is shown in Fig. 3. The housing is made of 5 mm thick PVDF with an outer layer of 30 mm thick glass-fiber-enforced epoxy. The anode is a 1 mm thick aluminum plate spot-welded onto a frame to avoid X-ray absorption in the anode. The cathode is nickel-coated solid brass. Both electrodes have a modified Chang profile. The effective length of the electrodes is 50 cm with a separation of 10 cm. The active discharge region is determined by collimating the X-ray emission with two lead apertures. The windows with clear apertures of 12 cm are made of CaF_2 with a diameter of 14 cm and 15 mm thickness. The rear mirror is a dielectric total reflection mirror. For the front mirror we use the reflection from the front window and the additional reflection from one uncoated Suprasil plate. The laser gas and the rail-gap gas are circulated through heat exchangers and filters by a water and gas management system to facilitate 1 Hz repetition rate operation.

2. Results and Discussion

2.1. Pulsed Power and Laser Performance

The laser was operated with a gas mixture of 4 mbar F_2, 160 mbar Kr and 4000–4500 mbar Ne. The output voltage of the Marx-bank was varied between 150 and 300 kV. For 275 kV Marx-output, the stored energy in the PFL is approximately 2 kJ at 340 kV and in the X-ray water capacitor it is approximately 360 J at 300 kV. The typical charging time of the PFL is 800 ns.

The temporal profiles of (a) the X-ray intensity, (b) the laser head voltage, (c) the discharge current, and (d) the laser emission are shown in Fig. 4 at 250 kV Marx-output. The X-ray emission profile was measured by a PIN diode (UDT PIN 10) protected by a thin aluminum foil from visible light. The laser head voltage was measured by a combination of a $CuSO_4$ solution voltage divider and a resistive voltage divider [15]. The current waveform was measured by a current-viewing-resistor of 0.0025 Ω (T & M Research Products Model No. W2K4-6.5S-0025). The optical output was measured by a biplanar vacuum photodiode (Hamamatsu R1193U-01). All signals were recorded on a 6 GHz digitizing oscilloscope (Tektronix 7250) in a shielded cabin.

The temporal profile of the X-ray emission is shown in Fig. 4a. The pulse width is 80 ns (FWHM) with a rise time of 20 ns (10–90%). The X-ray preionization starts 120 ns earlier than the main discharge. The voltage waveform in Fig. 4b shows fast ringing caused by the peaking capacitor and the laser head inductance. The inductance of the laser head calculated from the ringing period of 86 ns by considering the peaking capacitance of 6 nF and neglecting the resistive component is 33 nH which includes the inductance of the peaking capacitor. The inductance of the peaking capacitor was calculated as $L_p = 3$ nH. The geometrically determined laser head inductance L_h is strongly dependent on the gap distance d and is proportional to d^2 and was calculated as $L_h = 20$ nH [5, 16]. The

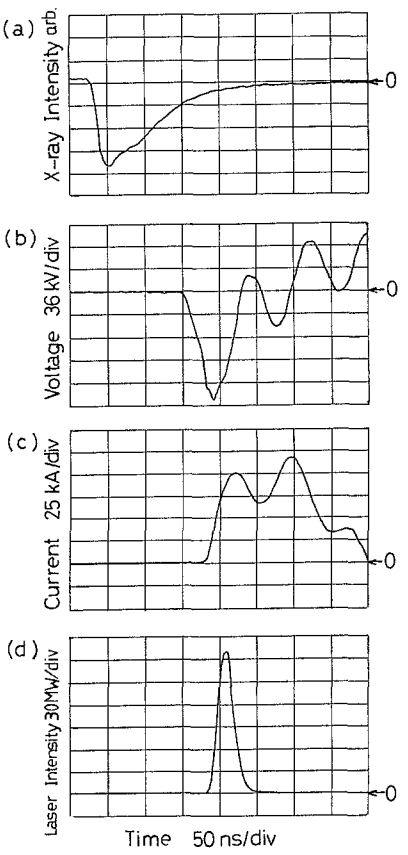

Fig. 4a–d. Typical pulse shapes of **a** the X-ray intensity, **b** the laser head voltage, **c** the discharge current, and **d** the laser intensity in case of laser total gas pressure of 4 bar. N_2 gas pressure in main rail-gap switch was 3 bar and in the X-ray rail-gap switch 3.5 bar. Output voltage of the Marx-bank was 250 kV

residual 10 nH inductance, which is the difference between the calculated one from the ringing time period and the geometrically determined one, is contributed by the time varying resistive component in the transient discharge. The breakdown voltage of the laser head is approximately 165 kV. The current waveform in Fig. 4c shows three peaks. However, effective pumping is obtained only at the first current peak (−100 kA) transiently. The electrical pumping power at the current peak is about 6.3 GW (1.6 MW/cm^3 considering a discharge volume of $10 \times 8 \times 50$ cm^3). The current risetime (10–90%) is 18 ns. The laser output in Fig. 4d shows a single peak corresponding to the first current peak. The pulse width of the laser is 28 ns (FWHM). The output energy was measured by a pyroelectric detector (Gentec ED-500). The maximum obtained laser energy was 4.7 J/pulse at a total pressure of 4500 mbar and 275 kV Marx-output. We show an overview of the operation parameters of this laser in Table 1.

2.2. Influence of Peaking Capacitance on Beam Width

The discharge width was observed to decrease with reduced peaking capacitance. The peaking capacitance was varied by changing the separation between the water-capacitor plates. The maximum capacitance is limited by

Table 1. Overview of the KrF amplifier

Geometrical cross section	10×10 cm^2
Repetition rate	1 pps[a]
Laser energy	4.7 J (PFL 340 kV charging)
Pumping power	2 MW/cc (PFL 340 kV charging)
Small signal gain coefficient	3%/cm[b]
Laser pulse width	28 ns (FWHM)
Laser head	
Active length	50 cm
Active cross-section	10×8 cm^2
Active volume	4 liter
Gas pressure	4 bar (F_2 4 mbar, Kr 160 mbar, Ne rest)
Rail-gap switch (main)	
Switch voltage	170–340 kV
Working gas	N_2/1–5 bar (abs.)
Repetition rate	1 pps[a]
Trigger	ArF laser[c]
Jitter tolerance	<5 ns (self-breakdown mode $\leqq 20$ ns)
Water capacitor (main)	Pulse-forming line/peaking capacitor
Capacitance	36 nF/6 nF
Transit time	48 ns/6 ns
Impedance	0.8 Ω/0.8 Ω
Preionization	X-ray (cold cathode type)
Repetition rate	1 pps[a]
Operation voltage	$\leqq 300$ kV
Storage capacitor	water capacitor/8 nF
Switch	rail-gap switch
Primary energy storage	5-stage Marx-generator
Charging voltage	75 kV/stage
Stored energy (max.)	4.2 kJ
Insulation	SF_6 gas
Repetition rate	1 pps

[a] Scheduled
[b] Minimum value, details will be reported elsewhere
[c] To be published elsewhere

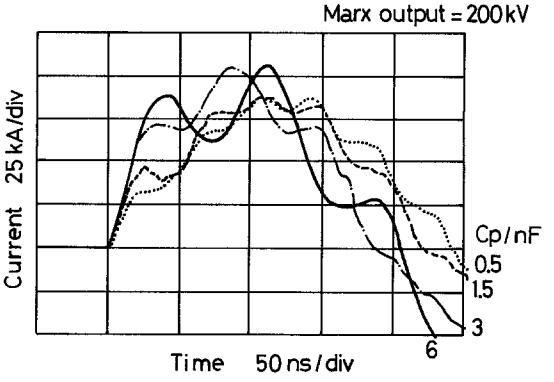

Fig. 5. Discharge currents with different peaking capacitances at Marx-bank output of 200 kV

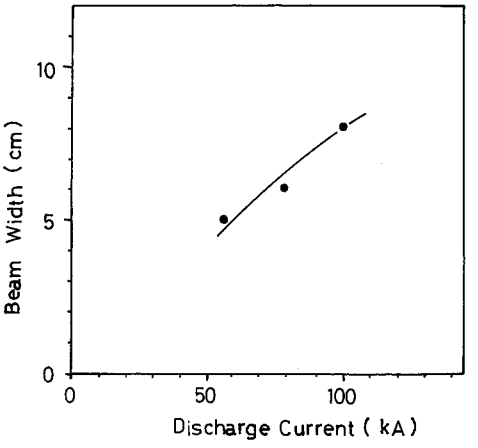

Fig. 6. Dependence of the discharge width on the peak discharge current at Marx-bank output of 250 kV

water breakdown. For 6 nF peaking capacitance, the distance between the plates is 2 cm with 6 ns double transit time.

In Fig. 5 the discharge current dependence on the peaking capacitance is shown. The output voltage of the Marx-bank was 200 kV, all other conditions were the same. At larger capacitance, the first current peak is larger with longer ringing period because of the larger peaking capacitance-head inductance time constant.

At smaller peaking capacitance, the current rise is determined by the total capacitance of the main PFL (36 nF) and the total inductance of the whole system including the rail-gap [5]. The resulting pumping power is then less than that required for the KrF excimer.

In Fig. 6 the dependence of the laser beam width on the peak current is shown. The photographic method described in the next section was employed in this measurement. The preionized width is limited to 10 cm by the pair of lead apertures already mentioned. However, the laser beam width is strongly dependent on the peak current within this preionized region. This effect has been also observed in a smaller device [17]. This is the result of the phenomena that with increased peak current, the minimum pumping power for the lasing is achieved in a broader area across the aperture.

2.3. *Beam Homogeneity*

The photographs shown in Fig. 7a, b are the fluorescence images of the KrF laser beam on graph paper. Both pictures were taken with open shutter but with different F-number aperture. The paper was kept 40 cm away from the output window. Figure 7a shows that the cross-section of laser output is about 10×8 cm. Figure 7b with lower exposure shows that the intense plateau region is about 10×5.5 cm. The beam profile shown in Fig. 7c was taken by using thermo-sensitive paper. There the image shows an intense plateau of approximately 10×5.5 cm. However, one should not forget the different threshold behavior of the two methods.

In Fig. 8 the spatial distribution of the laser pulse intensity is shown. The spatial dependence was measured with the same biplanar vacuum photodiode together with a 8 mm diameter aperture which was aligned at each of the positions A, B, C, D. The results show that there is no significant difference in pulse width at the measured

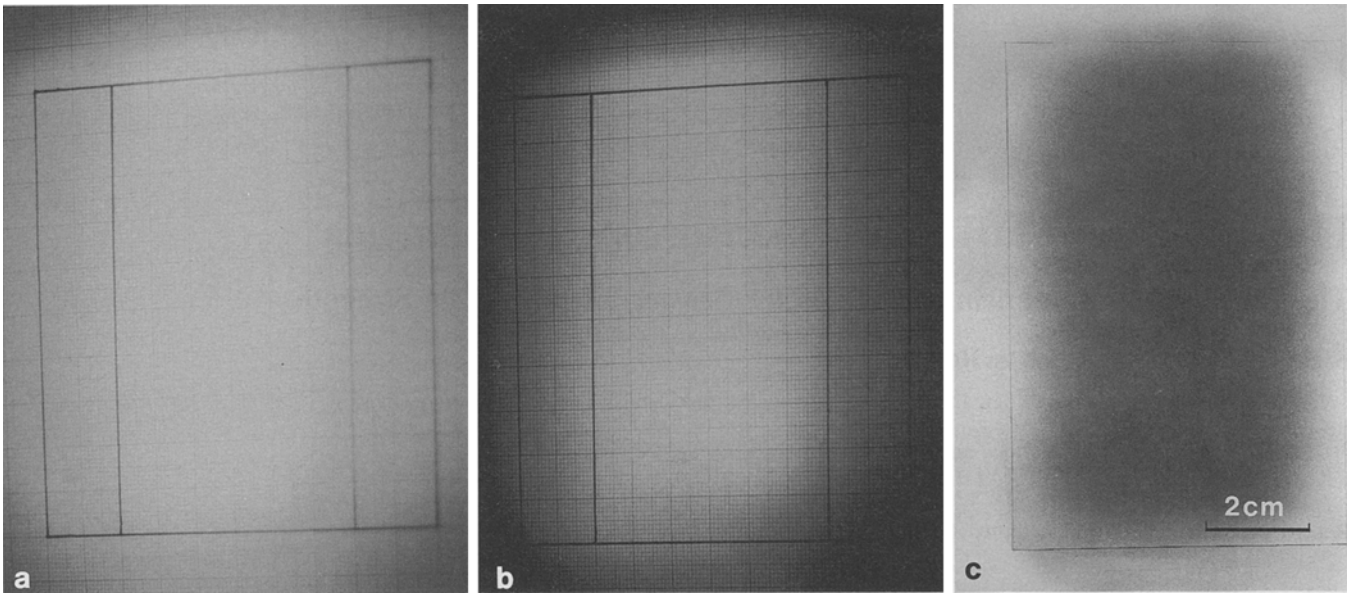

Fig. 7a–c. Observations of laser beam by **a** photograph of fluorescence image on graph paper, **b** same as **a** with smaller F-number, **c** beam image on thermo-sensitive paper. Total gas pressure 4 bar, N_2 gas pressure in the main rail-gap switch was 3 bar and in the X-ray rail-gap switch 3.5 bar, with 250 kV output voltage of the Marx-bank

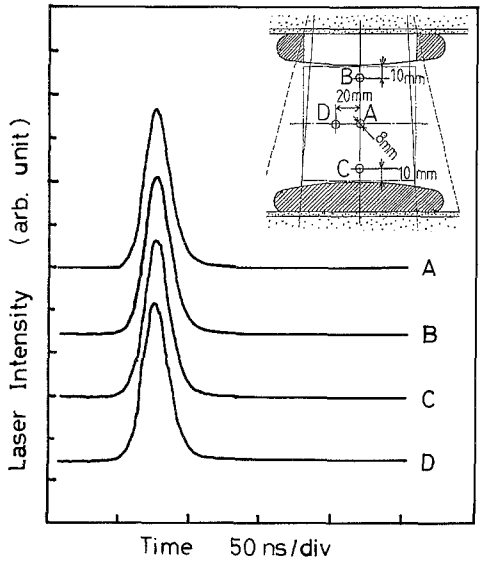

Fig. 8. Spatial dependence of the pulse duration in the laser beam. Output of the Marx-bank was 250 kV with F_2 4 mbar, Kr 160 mbar, Ne 4 bar

points. During the experiment, there was no spatially split lasing pattern observed. The stronger lasing region tended to be at the center with lower pumping power condition.

3. Conclusion

We have demonstrated a wide-aperture discharge-pumped KrF laser using a water dielectric pulse-forming line switched with a rail-gap together with a peaking-capacitor and collimated X-ray preionization. We have measured the influence of the peaking capacitance on the beam width and have obtained a laser beam cross-section of $10 \times 8\ cm^2$ with the intense plateau region being $10 \times 5.5\ cm^2$. The laser pulse energy was 4.7 J in a 28 ns pulse (FWHM).

Acknowledgements. The authors are indebted to Dr. M. Steyer for his suggestions on the basic design of the X-ray preionizer. One of us (H. Mizoguchi) acknowledges a research scholarship from Komatsu Ltd. This work has been supported by the Bunderministerium für Forschung und Technologie and by the Deutsche Forschungsgemeinschaft through its Leibniz program.

References

1. A. Endoh, M. Watanabe, N. Sarukura, S. Watanabe: Opt. Lett. **14**, 353 (1989)
2. A.J. Taylor, C.R. Tallman, J.P. Roberts, C.S. Lester, T.R. Gosnell, P.H.Y. Lee, G.A. Kyrala: Opt. Lett. **15**, 39 (1990)
3. S. Szatmári, F.P. Schäfer: J. Opt. Soc. Am. B **4**, 12 (1987)
4. T.S. Luk, A. McPherson, G. Gibson, K. Boyer, C.K. Rhodes: Opt. Lett. **14**, 1113 (1989)
5. L.F. Champagne, A.J. Dudas, N.W. Harris: J. Appl. Phys. **62**, 1576 (1987)
6. S. Watanabe, A. Endoh: Appl. Phys. Lett. **41**, 799 (1982)
7. B. Rácz, M. Steyer, H. Mizoguchi: Opt. Quantum Electron. (submitted)
8. W.J. Sarjeant, A.J. Alcock, K.E. Leopold: IEEE J. QE-**14**, 177 (1978)
9. R.S. Taylor, K.E. Leopold: Proc. 15th Power Modulator Symp., Baltimore, MD (1982) p. 113
10. R.S. Taylor, P.B. Corkum, S. Watanabe, K.E. Leopold, A.J. Alcock: IEEE J. QE-**19**, 416 (1983)
11. M. Steyer, B. Ouyang, K.A. Stankov, G. Szabó, H. Mizoguchi, F.P. Schäfer: Proc. SPIE **1023**, 75 (1989)
12. A. Endoh, S. Watanabe, M. Watanabe: J. Appl. Phys. **55**, 1322 (1984)
13. R.S. Taylor, K.E. Leopold: Rev. Sci. Instrum. **55**, 52 (1984)
14. M. Steyer: J. Phys. D **23**, 18 (1990)
15. W.J. Sarjeant, A.J. Alcock: Rev. Sci. Instrum. **47**, 1283 (1976)
16. B.L. Weyler, L.F. Champagne: SPIE Vol. **709**, 3 (1986)
17. M. Steyer, K.A. Stankov, H. Mizoguchi, B. Ouyang, F.P. Schäfer: Appl. Phys. B **49**, 331 (1989)